INTERNATIONAL JOURNAL OF OPTIMIZATION IN CIVIL ENGINEERING
Int. J. Optim. Civil Eng., 2026; 16(1):63-91

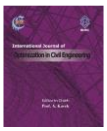

PERFORMANCE-BASED OPTIMIZATION OF STEEL FRAMES WITH CHEVRON LATERAL RESTRAINT SYSTEM AND SEMI-RIGID CONNECTIONS USING ADVANCED METAHEURISTIC OPTIMIZATION ALGORITHMS

K. Farzad[*, †] and M. Javanmard Barbin
Department of Civil Engineering, Ur.C., Islamic Azad University, Urmia, Iran

[DOI: 10.22068/ijoce.2026.16.1.663]

ABSTRACT

This study investigates the optimal design of steel frames with chevron bracing systems and semi-rigid connections using a performance-based design framework and metaheuristic optimization algorithms. Optimization effectively balances design performance and cost in structural engineering. The three algorithms employed were selected based on their proven application to similar optimization problems, enabling identification of the most suitable approach for the present case. Chevron bracing offers architectural benefits and enhances lateral stiffness and strength. However, unbalanced vertical forces from tension and compression braces under seismic loading require nonlinear analysis for reliable capacity estimation. To address this, pushover analyses with multiple lateral load patterns are performed to capture responses consistent with performance-based design principles. Connection behavior plays a decisive role in the global performance of steel frames. Conventional assumptions of rigid or pinned connections oversimplify reality and produce inaccurate predictions. In this study, semi-rigid connections are modeled with greater fidelity by incorporating column panel zones (CPZs) and gusset plate stiffness at bracing joints. CPZs significantly influence energy dissipation and deformation, while gusset plates may contribute up to 40% of connection rotational stiffness. Neglecting these effects can underestimate interstory drift and misrepresent hinge mechanisms. Results show that accounting for initial connection stiffness improves both accuracy and cost efficiency. For 10- and 15-story frames, structural cost were reduced by about 7%, underscoring the value of realistic connection modeling in optimal design.

Keywords: Braced steel frame; chevron bracing system; performance-based design; metaheuristic algorithms; semi-rigid connections.

Received: 11 December 2025; Accepted: 29 January 2026

[*]Corresponding author: Department of Civil Engineering, Ur.C., Islamic Azad University, Urmia, Iran
[†]E-mail address: keyvan.farzad@iau.ac.ir (K. Farzad)

1. INTRODUCTION

In engineering design, the primary objective is often to minimize project costs to the greatest extent possible. In structural engineering, this goal is pursued across different stages, including design, fabrication, and erection. The focus of optimal design is specifically on reducing costs during the design phase. In this context, performance-based design (PBD) has introduced a fundamental paradigm shift in structural engineering and has been recognized as a cornerstone of modern seismic design. Unlike traditional approaches that emphasize strength alone, PBD considers the actual behavior of structures, thereby enabling more precise control over safety, cost-efficiency, and post-earthquake functionality. Within this framework, structures are analyzed in the nonlinear domain to ensure that all performance objectives are satisfied at each stage of the design process. Acceptance criteria are formulated in terms of threshold values for both global structural responses and local member responses, depending on the selected performance levels and corresponding seismic hazard intensities. In recent years, the integration of PBD with optimization techniques and advanced metaheuristic algorithms has paved the way for a new generation of resilient, cost-effective, and performance-oriented structural systems.

With the advancement of engineering sciences and the growing demand for economic, safe, and efficient designs, optimization has emerged as a powerful tool in the structural design process. The objective of optimization in structural engineering is to identify the best combination of design parameters—such as cross-sectional dimensions, member configurations, and material types—that minimizes cost, weight, or deformation, or alternatively maximizes strength, efficiency, or safety, while simultaneously satisfying all design and code requirements. The need to achieve the most economical solutions in structural engineering problems has driven the development of structural optimization methods. In particular, the rapid evolution of metaheuristic optimization techniques has enabled the effective solution of highly complex structural optimization problems [1,2].

Building upon the advancements in structural optimization techniques, the effectiveness of these methods is strongly influenced by the choice of the lateral load-resisting system, which plays a decisive role in both structural performance and economic efficiency. Another critical consideration in the structural design stage is the selection of an appropriate lateral load-resisting system. Among the available options, steel chevron-braced frames have been widely adopted as a common seismic-resistant system due to their favorable ductility, efficient energy dissipation capacity, and high economic performance. These systems not only enhance the lateral stiffness of structures but also play a significant role in reducing inter-story drifts. Nevertheless, their nonlinear behavior can become highly complex under severe seismic excitations, particularly when semi-rigid connections are incorporated into the system [3].

A steel frame is essentially a planar assembly of linear members, such as beams and columns, interconnected through joints. These joints play a critical role in governing the overall structural response. From a structural standpoint, the properties of the connections significantly influence how the frame resists applied forces. Traditionally, the analysis and design of steel frames have been based on the assumption that beam-to-column joints behave either as idealized simple (pinned) or fully rigid connections. In a simple pinned connection, no moment is transferred between the beam and the column, and the joint is

[DOI: 10.22068/ijoce.2026.16.1.663]

capable of transmitting only shear and axial forces. Accordingly, the rotations of the connected members occur independently under loading. Conversely, in a fully rigid connection, no relative rotation occurs between adjacent members; the end moment of the beam is fully transferred to the column, and the angle between the beam and the column remains unchanged during frame deformations. Current structural analysis and design methods are largely rooted in these two idealized assumptions.

However, contrary to the classical "rigid or pinned" idealization, experimental and analytical investigations have shown that many practical connections exhibit *semi-rigid* behavior, characterized by finite rotational stiffness and a limited moment-transfer capacity. Beam-to-column joint deformations can adversely affect the stability of steel frames by increasing lateral drifts and reducing the effective stiffness of connected members. Therefore, accurate modeling of joint behavior is crucial for the design of steel frames, and explicitly accounting for semi-rigid connection behavior in structural analysis and design can lead to more reliable and economical solutions [4]. For this reason, modern design codes, such as AISC-LRFD [5], Eurocode 3 [6], and GB50017-2017 [7], recommend considering nonlinear effects in order to achieve more realistic predictions of structural response [8].

Given the complexity of semi-rigid connection behavior, their optimization has become a major challenge in structural engineering [9]. Semi-rigid joints exert a significant influence on the global behavior of steel frames and play a vital role in nonlinear design and performance-based assessments. Consequently, optimization of semi-rigid connections must be addressed not only at the local joint level but also in the context of the overall structural system. Due to the highly nonlinear and interdependent relationships among force, rotation, and stiffness, metaheuristic methods have gained wide application in solving semi-rigid connection optimization problems. These methods offer strong capabilities in exploring complex design spaces and identifying near-optimal solutions [8]. Ultimately, rigorous and realistic optimization of semi-rigid connections can lead to more cost-effective, safer, and practically feasible designs, while significantly enhancing the efficiency and performance of steel structures.

Valuable studies have been conducted on the precise analysis and optimization of semi-rigid connections. Since the 1980s, Machaly [10], Simoes [11], and Grierson [12] incorporated joint flexibility into the optimization process and concluded that considering semi-rigid connection effects can lead to a reduction in the structural weight of steel frames. However, the computational approaches employed in these studies were based on linear formulations, and their optimization methods demonstrated limited efficiency. To address these shortcomings, Kameshki and Saka [13,14] introduced nonlinear stiffness modeling combined with genetic algorithms for optimizing semi-rigidly connected structures under stability constraints. Hayalioglu and Degertekin [15,16] extended these efforts by incorporating different beam-to-column connection types and comparing the optimization outcomes across various connection properties. Nonetheless, their comparisons were restricted to a limited range of connection types, their computational models remained elastic, and the type of connection was not explicitly treated as a design variable. To overcome these limitations, Hagishita and Ohsaki [17] employed a modified plastic-hinge modeling approach and explicitly considered the type of connection as a design variable. Building on this direction, Bel Hadj Ali and colleagues [18] decomposed construction costs

[DOI: 10.22068/ijoce.2026.16.1.663]

into five components and proposed a more precise objective function. Hadidi and Rafiee [19] further advanced the field by including different connection types and beam/column sections as design variables and applying a hybrid optimization algorithm combining Harmony Search with the Big Bang–Big Crunch method. Subsequently, Artar and Daloglu [20,21] investigated six different beam-to-column connections with varying rotational stiffnesses and compared the performance of Genetic Algorithms and Harmony Search for structural optimization. In related studies, Shallan et al. [22] expanded the design variables by incorporating both semi-rigid beam-to-column and semi-rigid base connections, optimizing steel frames using Genetic Algorithms and Biogeography-Based Optimization. Truong and colleagues [23] extended optimization applications to three-dimensional as well as two-dimensional structures by employing advanced practical analysis and micro-genetic algorithms. Their later work [24] introduced probabilistic constraints into three-dimensional semi-rigid frame models, proposing optimized solutions under uncertainty. More recently, Deming et al. [8] proposed a two-stage optimization strategy for steel structures with semi-rigid connections. In their framework, traditional optimization techniques were first used to generate preliminary structural designs, which were then refined by incorporating a cost–performance rate model to improve suboptimal solutions. Further extending the scope of semi-rigid connection optimization, Yudong Qiu and colleagues [9] investigated steel frames with steel plate shear wall systems while accounting for semi-rigid connections. Additionally, Deming et al. [4] integrated construction-related costs of semi-rigid connections into their optimization framework, providing more realistic and implementable design solutions.

In this study, the optimization of steel chevron-braced frames is conducted by explicitly considering the actual behavior of beam-to-column connections, the influence of brace gusset plates on semi-rigid joint performance, and the effects of the column panel zone. The design framework is developed using well-established metaheuristic algorithms to achieve efficient and reliable solutions.

[DOI: 10.22068/ijoce.2026.16.1.663]

2. PERFORMANCE-BASED DESIGN OF STEEL CHEVRON-BRACED FRAMES

Performance-based design includes the following main stages:

2.1. Definition of performance objectives

The first step involves defining performance objectives, which are combinations of seismic hazard levels and corresponding structural performance expectations. Hazard levels range from low-intensity earthquakes with short return periods to high-intensity events with long return periods. Structural performance can be evaluated based on criteria such as physical damage or economic loss. In this study, following the guidelines of FEMA 356 [25] and ASCE/SEI 41-17 [26], three performance levels are defined: Immediate Occupancy (Uninterrupted Serviceability), Life Safety, and Collapse Prevention. These levels represent increasing degrees of structural demand and are used to evaluate the acceptability of the structural response under different seismic scenarios.

To accurately define performance objectives within a performance-based design

framework, it is essential to consider multiple seismic hazard levels. Typically, three primary hazard levels are employed:

- Hazard Level 1 – Operational-Level Earthquake (OLE): Represents a frequent, low-intensity event with a 50% probability of exceedance in 50 years (approximately 72-year return period).
- Hazard Level 2 – Design Basis Earthquake (DBE): Corresponds to a moderate seismic event with a 10% probability of exceedance in 50 years (475-year return period).
- Hazard Level 3 – Maximum Considered Earthquake (MCE): Represents a rare, high-intensity event with a 2% probability of exceedance in 50 years (2,475-year return period).

These hazard levels are used to correlate expected ground motions with targeted structural performance levels, thereby enabling a more rational and risk-informed design approach.

2.2. Determining the seismic capacity of the structure and its components through mathematical model analysis

Following the definition of performance objectives and the assessment of structural capacity, the next step involves evaluating whether the design meets the specified performance criteria. In this study, nonlinear static (pushover) analysis is employed to estimate the structural capacity and assess compliance with performance targets. Initially, the structure must demonstrate adequate performance under gravity loads and service-level conditions, in accordance with AISC-LRFD provisions [27]. Once these basic requirements are met, the structure is evaluated at each defined performance level through nonlinear analysis.

To simulate realistic load conditions during pushover analysis, gravity loads acting on the beams are determined based on the load combination $Q = 1{,}1(DL + 0{,}25\,LL)$ as recommended by FEMA 356. The target displacement for the analysis is also calculated in accordance with FEMA 356, using Equation (1),

$$\delta_t = C_0 C_1 C_2 C_3 S_a \frac{T_e^2}{4\,\pi^2} g \tag{1}$$

In this equation, T_e represents the effective fundamental period of the structure in the direction of analysis, and S_a is the spectral acceleration corresponding to T_e , determined for each performance level. In this study, S_a values are obtained based on a Soil Type D site classification, following the spectral response curves provided in Fig. 1 [1]. All additional coefficients and parameters required for the calculation are adopted as specified in the FEMA 356 guidelines.

The lateral force distribution pattern in the height of the building is according to formula (2):

$$C_{vx} = \frac{W_x h_x^k}{\sum_{i=1}^{n} W_i h_i^k} \tag{2}$$

[DOI: 10.22068/ijoce.2026.16.1.663]

Where w_i is the weight of the *i*th floor, h_i is the height of the *i*th floor, and k is calculated according to the following equation:

$$k = \begin{cases} 2 & for \quad T \geq 2{,}5\ seconds \\ 1 & for \quad T \leq 0{,}5\ seconds \end{cases} \tag{3}$$

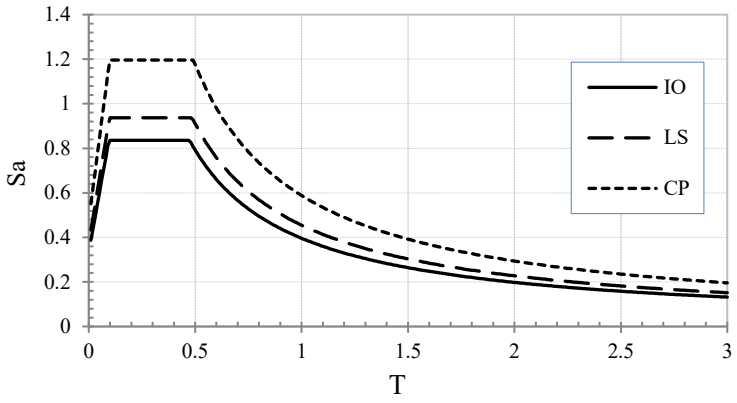

Figure 1: Response spectrum curve

For intermediate values of T, the value of k is calculated using interpolation.

FEMA 356 emphasizes that pushover analysis should be conducted using at least two different lateral load patterns to capture a range of structural responses. In this study, two lateral load patterns are employed: (1) a pattern based on the code coefficient C_{vx} (Formula 2), and (2) a uniform lateral load distribution proportional to the mass at each story level. To further account for the effects of higher vibration modes and improve the accuracy and practicality of the analysis, a modal pushover analysis approach is also utilized. This method combines the responses from multiple modes of vibration according to the modal combination procedure defined in Formula (4) [28].

$$F_j = \Sigma \alpha_n \Gamma_n m \phi_n S_n(\xi_n . T_n) \tag{4}$$

where α_n is the modal correction factor, which can take positive or negative values depending on the mode and structural characteristics; ϕ_n is the mode shape vector corresponding to the *n*th vibration mode; and S_n represents the spectral acceleration associated with the natural period of the *n*th mode. This formulation allows the modal pushover analysis to effectively incorporate the influence of multiple vibration modes on the lateral load distribution and resulting structural response and:

$$\Gamma = \frac{[\phi]^T [m]\{l\}}{M_n} \quad in\ which \quad M_n = [\phi]^T [m][\phi] \tag{5}$$

The responses received will be the maximum values provided by the three lateral load patterns above.

[DOI: 10.22068/ijoce.2026.16.1.663]

3. MODELING OF STEEL FRAMES WITH CHEVRON BRACING SYSTEM IN OPENSEES

In the structural design of steel frames, connections play a critical role in the overall system behavior. Accurate representation of their response—particularly their initial rotational stiffness—is essential in nonlinear analyses such as pushover analysis, where connection flexibility can significantly influence force and deformation demands [8,30]. To define the properties of semi-rigid connections in numerical modeling, the initial rotational stiffness K_θ must be determined. The initial rotational stiffness is defined as the slope of the moment–rotation (M–θ) curve at very small rotations. This stiffness characterizes the linear elastic range of the connection and directly affects the lateral stiffness, natural frequencies, and interstory drift of the frame. The determination of initial rotational stiffness can be based on experimental results, empirical and analytical models, or design standards. For instance, design codes such as Eurocode 3 Part 1-8 classify connections according to the following criteria:

$$\begin{cases} if \quad K_\theta \geq 25\frac{E,I_b}{L_b} & \text{Rigid connection} \\ if \quad K_\theta \leq 0{,}5\frac{E,I_b}{L_b} & \text{Pinned connection} \\ \text{Otherwise Semi} - \text{rigid connection} \end{cases} \tag{6}$$

According to studies by Moghaddam & Sadrara [30,31], Qin et al. [32], Zhang et al. [33], Azizinamini et al. [34], and Brown & Anderson [35], the initial rotational stiffness of semi-rigid connections typically ranges between 1000 kN/rad and 300,000 kN/rad. In this study, the OpenSees platform is employed for finite element modeling and pushover analysis of the steel frames under investigation. Pushover analysis, conducted through the gradual application of lateral loads until the yielding mechanism is reached, enables the evaluation of deformation distribution, the formation of plastic hinges, and the identification of structural weaknesses. In steel frames with chevron bracing systems, the seismic performance is strongly influenced by the behavior of beam-to-column connections as well as the interaction between braces and beams. In such systems, unfavorable performance of the compressive brace may lead to adverse phenomena such as the development of counteracting forces in the beam, the occurrence of the Vierendeel mechanism, and concentration of deformations within the connections. Therefore, it is of paramount importance to consider the actual nonlinear behavior of semi-rigid connections, to accurately model the column panel zone, and to account for the stiffness contribution of gusset plates to the overall beam-to-column joint stiffness. According to established guidelines such as FEMA 356, FEMA 350, and ASCE/SEI 41-17, independent and nonlinear modeling of joint components, including beam-to-column connections and panel zones, is recognized as a fundamental requirement for nonlinear structural analysis.

[DOI: 10.22068/ijoce.2026.16.1.663]

3.1. Modeling of linear elements in steel frames with chevron bracing system using OpenSees

In the nonlinear modeling of beams and columns within OpenSees, distributed plasticity is represented using nonlinear beam-column elements with fiber sections. This approach, as opposed to plastic hinge idealization at discrete nodes, allows for the possibility of yielding to occur not only at the member ends but also along the entire length. In the analytical models of the studied frames, P–Δ effects are incorporated for all elements through the use of corotational geometric transformations. For material modeling, the beam and column fibers are assigned a bilinear constitutive model with a post-yield hardening ratio of 3% of the elastic modulus, in order to capture nonlinear material behavior. The modeling of inelastic brace behavior is considerably more complex, as it requires accounting for the interaction of yielding, global buckling, local buckling, and fracture. One common method is the axial-flexural fiber model, which necessitates calibration against experimental results to determine parameters such as the appropriate number of elements per brace, initial mid-length imperfections, and material hardening ratios. Alternatively, brace behavior can be modeled using a phenomenological approach, as proposed by Jain and Goel [36], which has also been validated by FEMA. In this method, brace responses under tension and compression are modeled according to the characteristic hysteretic curves (see Fig. 2), where the post-buckling compressive strength is typically taken as 20% of the initial buckling load, in line with FEMA recommendations. Within OpenSees, the Steel01 material model is employed to represent the constitutive behavior of beams and columns, while uniaxialMaterial Hysteretic is used to capture the nonlinear hysteretic response of braces.

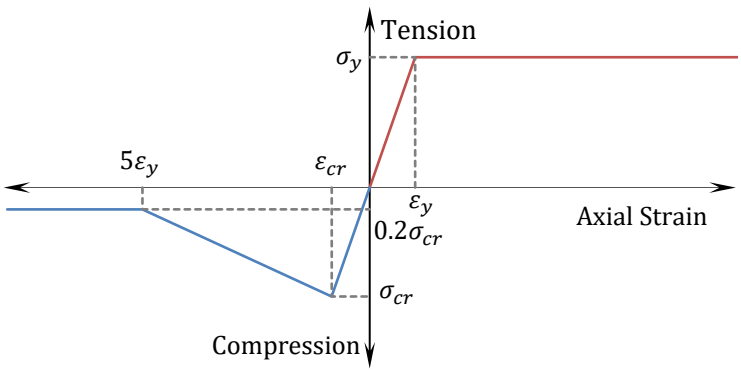

Figure 2: Stress–Strain Curve of Brace Behavior

3.2. Modeling of the column panel zone in OpenSees

Accurate modeling of Column Panel Zones (CPZs) in the nonlinear analysis of steel frames is essential due to their significant contribution to connection deformations and energy dissipation under lateral loads. The panel zone, defined as the web area of the column bounded by the flanges of the beam and column, undergoes substantial shear deformation during strong ground motions or large inelastic drifts. Neglecting this deformation may result in underestimation of inter-story drifts and overestimation of beam plastic rotations, thereby misrepresenting the actual structural performance and failure mechanisms [37].

[DOI: 10.22068/ijoce.2026.16.1.663]

Research has shown that panel zones may yield and dissipate energy under seismic loading, particularly in deep columns and weak panel configurations [38,39]. Assuming the panel zone to be rigid oversimplifies the behavior, leading to an inability to predict shear strain concentrations and incorrect localization of plastic hinges. Therefore, for performance-based seismic design of steel frames, proper modeling of CPZs is necessary to achieve reliable predictions of system behavior, damage states, and collapse potential [40]. In finite element models, panel zones can be represented using zeroLength shear springs with nonlinear material properties [41].

3.3. Modeling of semi-rigid connections in OpenSees

Accurate modeling of semi-rigid connections is essential in nonlinear analyses such as pushover analysis. For this purpose, OpenSees provides a powerful platform that enables advanced simulation of connections, incorporating material nonlinearities, hysteretic behavior, local buckling, and other complex parameters. In OpenSees, semi-rigid connections are typically modeled using concentrated rotational springs placed at the beam-to-column interface. The most common approach involves the use of ZeroLength elements along the rotational degree of freedom (DOF 3), where a nonlinear uniaxial material model such as Steel01 or Hysteretic is assigned to capture the flexural properties of the connection. This method offers several advantages, including simplicity in numerical implementation, the ability to define initial stiffness, ultimate strength, and post-yield or strength degradation characteristics, as well as the capability to model the cyclic hysteresis of connections under reversed loading. Numerous studies, such as those by Kishi & Chen (1990) [42] and Jaspart (1997) [43], have investigated the behavior of semi-rigid connections and proposed empirical formulations for their parameters. Moreover, design codes such as Eurocode 3 (EC3) and AISC 360-16 classify connections according to their rotational stiffness. In this study, semi-rigid connections of the steel chevron-braced frame are modeled in OpenSees using rotational spring elements to assess their influence on the nonlinear structural response, including displacements, load-bearing capacity, and failure mechanisms. Fig. 3. illustrates the details of the beam-to-column connection modeling in OpenSees.

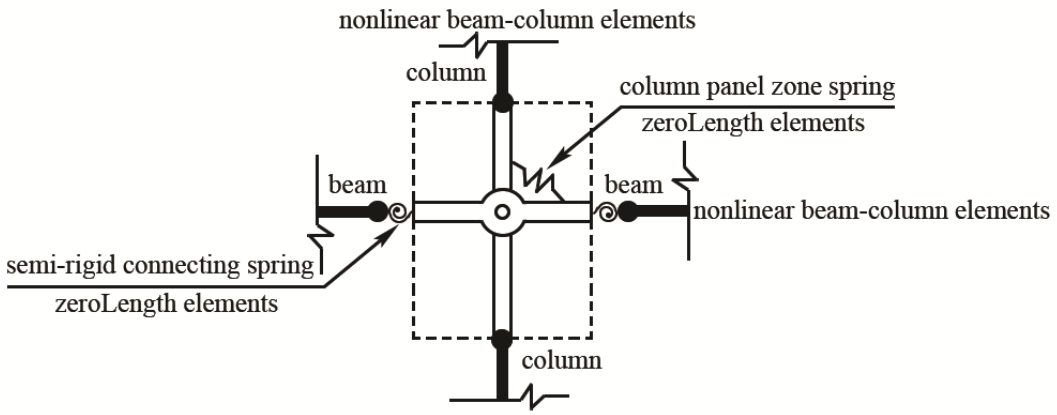

Figure 3: Details of beam-to-column connection modeling in OpenSees

[DOI: 10.22068/ijoce.2026.16.1.663]

3.4. Effect of gusset plate stiffness on beam-to-column connection stiffness

In steel frames with bracing systems, gusset plates play a key role in transferring forces among beams, columns, and braces. These plates are often neglected in conventional analyses, although they can contribute significantly to the overall stiffness of the connection. Studies have shown that the rotational stiffness provided by gusset plates may account for 20–40% of the total connection stiffness [44]. Therefore, neglecting this component can lead to reduced modeling accuracy, misestimation of lateral stiffness, and incorrect prediction of frame hinging mechanisms. Consequently, it is recommended that gusset plates be explicitly incorporated into nonlinear analyses, typically represented as separate rotational springs. For numerical modeling of gusset plate effects in nonlinear analysis using OpenSees, a common approach is to employ ZeroLength elements with an equivalent spring material. The gusset plate stiffness can be represented as a rotational spring, derived according to the following mechanical relationships:

A) Equivalent Rotational Stiffness of Gusset Plates [45]:
In this modeling approach, the gusset plate is idealized as a bending beam or plate. When the plate length is relatively large and its thickness is small (the most common real-world condition), this method provides a reliable representation of gusset plate behavior and is calculated by equation 7.

$$K_{\theta.gusset} = \frac{E, I_{gp}}{L_{gp}} \tag{7}$$

where E is the elastic modulus of steel, I_{gp} is the moment of inertia of the gusset plate, and L_{gp} is the effective length of the gusset plate.

B) Equivalent Shear Stiffness of Gusset Plates [46]:
In this modeling approach, it is assumed that the major deformation originates from the shear of the gusset plate. This method is most appropriate for short and thick plates with a low length-to-thickness ratio and is calculated by equation 8.

$$K_{\theta.gusset} = \frac{k_s, G, A_s}{L_s} \tag{8}$$

where G is the shear modulus of steel, A_s is the effective shear area of the gusset plate, and $k_s \approx 0{,}8$ is the shear correction factor. Depending on the geometry, connection configuration, and load transfer mechanism, different modeling assumptions may govern the calculation of gusset plate stiffness. However, according to most experimental and numerical studies, the flexural model is usually considered the governing model for determining the rotational stiffness of gusset plates in semi-rigid connections. After computing the effective gusset plate stiffness, it is combined with the semi-rigid beam-to-column connection stiffness according to Equation 9 [47]:

$$K_{\theta.total} = K_{\theta.joint} + K_{\theta.gusset} \tag{9}$$

[DOI: 10.22068/ijoce.2026.16.1.663]

Studies indicate that neglecting gusset plate stiffness may lead to inaccurate estimation of the lateral stiffness of the frame and misrepresentation of failure mechanisms. This effect is particularly critical in pushover or dynamic analyses.

4. METAHEURISTIC ALGORITHMS

Metaheuristic algorithms have been extensively applied to engineering problems due to their high flexibility, global search capability, and relatively low computational cost. Unlike traditional optimization methods, these algorithms are not restricted to specific problem types and can be effectively employed across a wide range of complex, nonlinear, and high-dimensional optimization tasks. Each metaheuristic algorithm employs a unique search strategy and formulation to explore the solution space and converge toward a global optimum. In this study, three widely used metaheuristic algorithms—previously validated in similar structural optimization research—are employed to optimize of steel frame structures. In this study, three metaheuristic algorithms—described in detail in this section—are utilized to optimize both the the cross-sectional properties of chevron braced steel frame and initial rotational stiffness of semi-rigid connections. Based on their respective formulations, these algorithms have demonstrated the capability to effectively address the types of complex optimization problems investigated in this research[9,48,49].

4.1. Modified Dolphin Echolocation algorithm (MDE)

Many human-developed technologies are inspired by natural processes. Dolphins, regarded as one of the most intelligent species after humans, use acoustic localization as a form of biological sonar to detect and track prey. Drawing inspiration from this behavior, the dolphin echolocation algorithm simulates the search process within a design space, mimicking the way dolphins use echolocation to explore and identify optimal hunting paths[50].
The main steps of MDE are as follows:

Step 1. Set random location coordinates for the dolphin.

Step 2. Using Eq.10 , the predefined probability (PP) assigned to the responses was determined.

$$\mathrm{PP}(\mathrm{L}_i) = PP_1 + (1 - PP_1)\frac{\mathrm{L}_i^{Power}}{(LoopsNumber)^{power} - 1} \tag{10}$$

where $\mathrm{PP}(\mathrm{L}_i)$ is a predefined probability in step i , PP_1 is predetermined probability in step one, L_i is the current step number, and *LoopsNumber* is the number of steps in which the algorithm must achieve the optimal solution.

Step 3. Calculate the fitness of each dolphin.

[DOI: 10.22068/ijoce.2026.16.1.663]

Step 4. The fitness of each location is distributed to its neighbors using a symmetric triangular distribution or another symmetric distribution.

Step 5. All devoted fitness values are added to each variable at every location to compute the accumulative fitness (AF). The cumulative fitness for variable *j* at position *i* is obtained using the following equation:

$$\mathrm{AF}_{(\mathrm{A+k})\mathrm{j}} = \frac{1}{R_e}(R_e - |K|) * \ \mathrm{Fitness(i)} + \mathrm{AF}_{(\mathrm{A+k})\mathrm{j}} \tag{11}$$

R_e is the effective radius.
where $\mathrm{AF}_{(\mathrm{A+k})\mathrm{j}}$ is cumulative fitting, and A refers to the option chosen for the variable j located in i position. The value of k also varies from $-R_e$ to R_e. R_e is defined as an effective radius within which the cumulative fitness around A is influenced by its own fitness. In the modified dolphin echolocation algorithm, R_e is set to one-quarter of the search range for the corresponding variable.

Step 6. A small value ε is added to the accumulative fitness (AF) matrix to prevent premature convergence to local optima. The choice of ε depends on the definition of fitness and is preferably less than or equal to the minimum possible fitness value.

$$\varepsilon = AF + \ \varepsilon \tag{12}$$

Step 7. Find the best location achieved and set its AF to zero.

Step 8. Calculate the probability by normalizing AF as:

$$P_{ij} = \frac{AF_{ij}}{\sum_{i=1}^{LAj} AF_{ij}} \tag{13}$$

where P_{ij} is the probability of the *i*th alternative to appear in the *j*th dimension. AF_{ij} is the accumulative fitness of the *i*th alternative to be in the *j*th dimension.

Step 9. Select $\mathrm{PP(L}_i\mathrm{)}$ percent of next step locations from best location dimensions. Distribute other values according to P_{ij} .

Step 10. Repeat steps 2–9 for as many times as the Loops Number is.

4.2. Center of mass optimization algorithm (CMO)

The Center of Mass Optimization (CMO) algorithm is inspired by the physical principle of the center of mass and is designed to solve complex optimization problems with high efficiency using only a single tuning parameter. In this algorithm, search agents are assigned mass values proportional to their fitness, and agents with greater mass exert a stronger influence on the system, attracting others toward the center of mass. Conversely, agents with lower mass are more influenced by the movement of others. This mass-based interaction

[DOI: 10.22068/ijoce.2026.16.1.663]

forms the foundation of the search mechanism within the design space [48]. In the CMO algorithm, the mass of each search agent is calculated from the following equation:

$$m_i = \frac{1}{fit_i} \tag{14}$$

where fit_i is the fitness value of the objective function for the *i*th agent position.
In the CMO algorithm, search agents are classified into two groups based on their fitness: higher-quality agents (larger masses) and lower-quality agents (smaller masses). Each superior agent is then updated by considering its interaction with an inferior agent, specifically based on the distance between them. This mechanism promotes both exploration and exploitation of the design space by simulating gravitational-like attraction influenced by fitness-based mass differentiation.

For each pair of particles in the *l*th iteration and for each *i*th agent, the position of the center of mass (X^C) and the inter-particle distance (Dl) are calculated using the following expressions:

$$X_i^C(l) = \frac{m_i X_i(l) + m_{\frac{nop}{2}+i} X_{\frac{nop}{2}+i}(l)}{m_i + m_{\frac{nop}{2}+i}}, \quad i = 1,2,\dots,\frac{nop}{2} \tag{15}$$

$$Dl_i(l) = \left| X_i(l) - X_{\frac{nop}{2}+i}(l) \right|, \quad i = 1,2,\dots,\frac{nop}{2} \tag{16}$$

where *nop* represents the number of particles.

One of the most important characteristics of the CMO algorithm is its ability to maintain a balance between exploration and exploitation throughout the optimization process. Initially, the algorithm emphasizes exploration to broadly search the design space, while over successive iterations, the focus gradually shifts toward exploitation to refine the solution near optimal regions. In the CMO algorithm, particle positions are updated using the following formulation:

In the first step, a control parameter (CP) is introduced, which gradually decreases from 1 to 0 over the course of the optimization process.

$$CP(l) = exp\left(-\frac{5l}{l_{max}}\right) \tag{17}$$

where l_{max} is the maximum number of optimization iterations.
If the value of Dl_i exceeds the control parameter CP, the position of the *i*th particle pair is updated in the exploration phase according to the following equation:

$$X_i(l+1) = X_i(l) - r.\left(X_i^C(l) - X_i(l)\right) + r.\left(X_{best}(l) - X_i(l)\right) \tag{18}$$

$$X_{\frac{nop}{2}+i}(l+1) = X_{\frac{nop}{2}+i}(l) + r.\left(X_i^C(l) - X_{\frac{nop}{2}+i}(l)\right) + r.\left(X_{best}(l) - X_{\frac{nop}{2}+i}(l)\right) \tag{19}$$

[DOI: 10.22068/ijoce.2026.16.1.663]

If the value of Dl_i is less than the control parameter CP, the position of the *i*th particle pair is updated during the exploitation phase using the following expression:

$$X_i(l+1) = X_i(l) + r.\left(X_i(l) - X_{\frac{nop}{2}+i}(l)\right) \tag{20}$$

$$X_{\frac{nop}{2}+i}(l+1) = X_{\frac{nop}{2}+i}(l) + r.\left(X_i(l) - X_{\frac{nop}{2}+i}(l)\right) \tag{21}$$

In the above expressions, *r* represents a uniformly distributed random number between 0 and 1, and X_{best} denotes the best solution identified up to the current iteration.

4.3. Modified Newton Metaheuristic Algorithm (MNMA)

The Newton Metaheuristic Algorithm (NMA) [51] is a population-based optimization algorithm inspired by the Newton gradient iteration scheme. In this approach, a population of n agents is randomly initialized within the design space of the optimization problem. At each iteration, the algorithm requires numerical approximations of the derivatives of the objective function in order to update the population positions. Accordingly, the objective function values of all individuals are evaluated, and the population is ranked in ascending order of the objective values. For a discrete optimization problem, the position of the *i*-th search agent at iteration *t* is updated as follows:

$$X_i^{t+1} = X_i^t + \Delta X_i^t \tag{22}$$

$$\Delta X_i^t = round\left(\left(\frac{t}{t_{max}}\right).R_1^t.\Gamma.(X_{i-1}^t - X_{i+1}^t) + \left(1 - \frac{t}{t_{max}}\right).R_2^t.(X_B - X_i^t)\right) \tag{23}$$

$$\Gamma = \frac{\kappa^2\phi(X_{i+1}^t) + (1-2\kappa)\phi(X_i^t) - (1-\kappa)^2\phi(X_{i-1}^t)}{2\kappa\phi(X_{i+1}^t) - 2\phi(X_i^t) + 2(1-\kappa)\phi(X_{i-1}^t)} \tag{24}$$

$$\kappa = \frac{\|X_i^t - X_{i-1}^t\|}{\|X_{i+1}^t - X_{i-1}^t\|} \tag{25}$$

where R_1^t and R_2^t are vectors of random numbers uniformly distributed in [0,1], t_{max} is the maximum number of iterations, and X_B represents the best solution found so far.

The Modified Newton Metaheuristic Algorithm (MNMA) [49] is an extended variant of NMA implemented in a sequential manner using the External Penalty Function Method (EPFM) to handle design constraints. In the first stage of MNMA, an initial population of n individuals is generated randomly, and NMA is executed with a small penalty parameter r_p. Due to the small penalty value, the algorithm may converge toward an infeasible solution.

In the second stage, a new population is generated in the neighborhood of the best solution X_B obtained from the previous stage. Specifically, X_B is directly carried over to the new population, while the remaining individuals are sampled randomly as follows:

$$X_i = F_N(X_B, \sigma X_B) \tag{26}$$

[DOI: 10.22068/ijoce.2026.16.1.663]

where F_N denotes a normal distribution with mean X_B and standard deviation σX_B. The penalty parameter is updated at each stage according to:

$$r_p = \gamma r_p \tag{27}$$

The convergence rate of MNMA is influenced primarily by parameters σ and γ, whose recommended values are 0.1 and 10, respectively, as determined by sensitivity analysis. The optimization process continues until one of the stopping criteria is satisfied.

5. FORMULATION OF THE PERFORMANCE-BASED DESIGN PROBLEM FOR CHEVRON-BRACED STEEL FRAMES WITH SEMI-RIGID CONNECTIONS

Given the complexities arising from geometric nonlinearities, material characteristics, and the semi-rigid nature of connections, the adoption of performance-based optimization approaches for the design of steel chevron-braced frames with semi-rigid beam-to-column connections is indispensable. In this paradigm, the structural design is performed to satisfy prescribed performance objectives (e.g., limits on interstory drifts, formation of plastic hinges at controlled locations, or a target damage level for the design earthquake) while simultaneously minimizing an objective function such as total weight or cost. The optimization problem in this framework is a multivariable nonlinear program whose design variables typically include member cross-section dimensions and the rotational stiffness of semi-rigid connections, subject to a set of code and performance constraints. The primary goal is to find a set of design variables that minimizes the weight or construction cost of the structure while satisfying the governing constraints. A performance-based optimization formulation for a chevron-braced steel frame with semi-rigid connections can be stated as follows [9]:

$$C(x) = C_\rho \left(\sum_{i=1}^{ne} \rho A_i L_i + \sum_{j=1}^{nc} C_j^c \right) \tag{28}$$

where the connection construction cost C_j^c is modeled following Truong [52] as:

$$C_{R_i}^c = 0{,}125 \rho A_b L_b \left(1 + 1{,}8 \frac{R_i - R_i^L}{R_i^U - R_i^L} \right) \tag{29}$$

$$subject\ to: \qquad g_i^s(x) \leq 0 \,, \quad i = 1.2. \ldots .n \tag{30}$$

$$g_j^{PBD}(x) \leq 0 \,, \quad i = 1.2. \ldots .n \tag{31}$$

In the above expressions, C denotes the total construction cost, C_ρ is the unit cost per unit weight of steel, ne is the number of members, ρ is the material density, A_i and L_i are the

[DOI: 10.22068/ijoce.2026.16.1.663]

cross-sectional area and length of member i, respectively, nc is the number of semi-rigid connections, and C_j^c is the cost associated with connection j computed by Eq. (29). In Eq. (29), R_i is the initial rotational stiffness of the connection, A_b and L_b are the area and length of the beam connected to the joint, and R_i^L and R_i^U are the lower and upper bounds for the range of permissible initial rotational stiffness values for the connections. The constraints g_i^s represent standard design/code constraints (e.g., strength, stability, serviceability), applied in accordance with ANSI/AISC 360-22 [27], while g_j^{PBD} denote performance-based constraints (e.g., drift limits, connection rotation limits, formation sequence of plastic hinges).

The allowable inter-story drift limits for various performance levels are determined using the following formula:

$$g_1 = \frac{\Delta^i}{(\Delta^i)_{all}} - 1 \leq 0 \qquad i = IO \text{ ، } LS \text{ ، } CP \tag{32}$$

where Δ is the inter-story drift, and $(\Delta)_{all}$ is the allowable inter-story drift for each performance level as specified in FEMA-356, presented in Table 1 [25,26].

Table 1: Permissible values of floor drift

Performance level	$(\Delta)_{all}$
IO	0.5%
LS	1.5%
CP	2%

The possible failure mechanisms in beams, according to FEMA-356, are deformation-controlled (DC) actions at various performance levels. The acceptance criteria are determined based on the plastic rotation capacity of the beams, as expressed in Formula 33.

$$g_2 = \frac{\theta^i}{(n\theta_y)} - 1 \leq 0 \qquad i = IO \text{ ، } LS \text{ ، } CP \tag{33}$$

where θ is the plastic rotation of the beam at each performance level, n is a coefficient determined from Table 5-6 of FEMA-356 based on the compactness classification of the steel sections, and θ_y is the yield rotation calculated using Formula 34.

$$\theta_y = \frac{ZF_{ye}l_b}{6EI_b} \tag{34}$$

where Z is the plastic section modulus, F_{ye} is the expected yield stress of the steel, l_b is the member length, and E is the modulus of elasticity.

The acceptance criteria for columns in performance-based design are defined based on controlling the possible failure mechanisms within the column. To accomplish this, force-controlled (FC) and deformation-controlled (DC) actions must be identified at various

[DOI: 10.22068/ijoce.2026.16.1.663]

performance levels. Columns subjected to bending moments, in which the axial force at the target displacement is less than 50% of the lower limit compressive strength P_{CL}, are classified as deformation-controlled (DC). In such cases, the maximum allowable plastic rotation for each column is defined as follows:

$$g_{DC.i}^{p/50}(X) = \frac{\theta_i^{p/50}}{\theta_{p.i}^{p/50}} - 1 \leq 0 \,.\, i = 1.2. \ldots . nc \tag{35}$$

where $\theta_i^{p/50}$ is the maximum plastic rotation of the *i*th column at the risk level $p/50$, and $\theta_{p.i}^{p/50}$ is the allowable plastic rotation of the *i*th column, defined according to Table 5-6 of FEMA 356, based on the axial force and seismic compression conditions of the steel section. Here, *nc* represents the total number of columns.

Columns subjected to combined bending and shear forces at a target displacement greater than or equal to 50% of the column's lower limit compressive strength P_{CL} are classified as force-controlled. For these columns, the maximum plastic rotation constraint is defined as follows:

$$g_{FC.i}^{p/50}(X) = \frac{P_{UF.i}^{p/50}}{P_{CL}} + \frac{M_{UF.i}^{p/50}}{M_{CL}} - 1 \leq 0 \,.\, i = 1.2. \ldots . nc \tag{36}$$

where $P_{UF.i}^{p/50}$ and $M_{UF.i}^{p/50}$ represent the axial and moment forces, respectively, acting on the *i*th column due to gravity loads combined with seismic forces under force-controlled conditions at the hazard level $p/50$. P_{CL} and M_{CL} denote the lower limit compressive strength and flexural strength of the column, respectively.

The axial deformation constraint for braces is defined as follows:

$$g_{\Delta.i}^{p/50}(X) = \begin{cases} \dfrac{\Delta_{Ci}^{p/50}}{\Delta_{PCi}^{p/50}} - 1 \leq 0 & in\ compressin \\ \dfrac{\Delta_{Ti}^{p/50}}{\Delta_{PTi}^{p/50}} - 1 \leq 0 & in\ tension \end{cases} .\, i = 1.2. \ldots . nb \tag{37}$$

where $\Delta_{Ci}^{p/50}$ and $\Delta_{Ti}^{p/50}$ are the axial deformations of the *i*-th brace for the hazard level $p/50$ in compression and tension, respectively; $\Delta_{PCi}^{p/50}$ and $\Delta_{PTi}^{p/50}$ are their allowable values according Table 5-6 of FEMA 356; and nb is the number of braces.

For controlling the axial deformation of columns in tension, Equation (37) is also used. In this study, construction-related constraints are also considered. The constraint related to the beam-to-column connection, as shown in Fig. 4. is applied according to Equation (38), and the constraint related to the column-to-column connection between stories is expressed by Equation (39):

[DOI: 10.22068/ijoce.2026.16.1.663]

$$g_{B1} = \frac{b_{fb}}{b_{fc}} - 1 \leq 0 \text{ ، } \qquad m = 1 \text{ ، } \ldots \text{ ، } nj \tag{38}$$

$$g_c = \frac{A_c^T}{A_c^B} - 1 \leq 0 \tag{39}$$

where A_c^B is the cross-sectional area of the lower-story column and A_c^T is the cross-sectional area of the upper-story column.

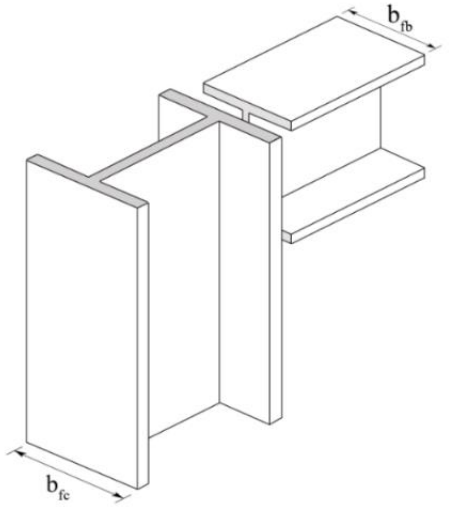

Figure 4: beam-to-column connection

6. NUMERICAL EXAMPLES

The structures investigated in this study are 5-bay steel frames with 10 and 15 stories, with bay lengths equal to 5 meters and story heights of 3 meters. The grouping of members in these structures is such that the exterior and interior columns are placed in two different groups over two consecutive stories. The grouping of beams, braces, and connections is performed similarly to the columns over two consecutive stories, as shown in Fig. 5. The cross-sections of beams and columns are selected from the standard W-section list, and the brace cross-sections are selected from the HSS box section list, according to Table 2. The values of the applied dead and live loads on the beams are 24.5 kN/m and 25.5 kN/m, respectively. The yield stress of the beam, column, and brace elements is 235 MPa, with a strain hardening ratio of 3%. The unit weight of steel and the modulus of elasticity are considered to be 76.82 kN/m³ and 200 GPa, respectively. In the optimization process of steel frames with chevron bracing systems and semi-rigid connections, the initial rotational stiffness of the connections is first considered as one of the design variables, ranging from 1000 kNm/rad to 300,000 kNm/rad. Then, for comparison and to examine the necessity of considering beam-to-column connections, the optimization process is repeated for rigid beam-to-column connections. Considering the discrete nature of the design space of steel frames, 31 values of initial rotational stiffness of connections are used within the range of 1000 to 300,000 with equal intervals of 1000. The construction costs of columns, beams,

[DOI: 10.22068/ijoce.2026.16.1.663]

and braces are assumed to be 1300 USD per ton [9].

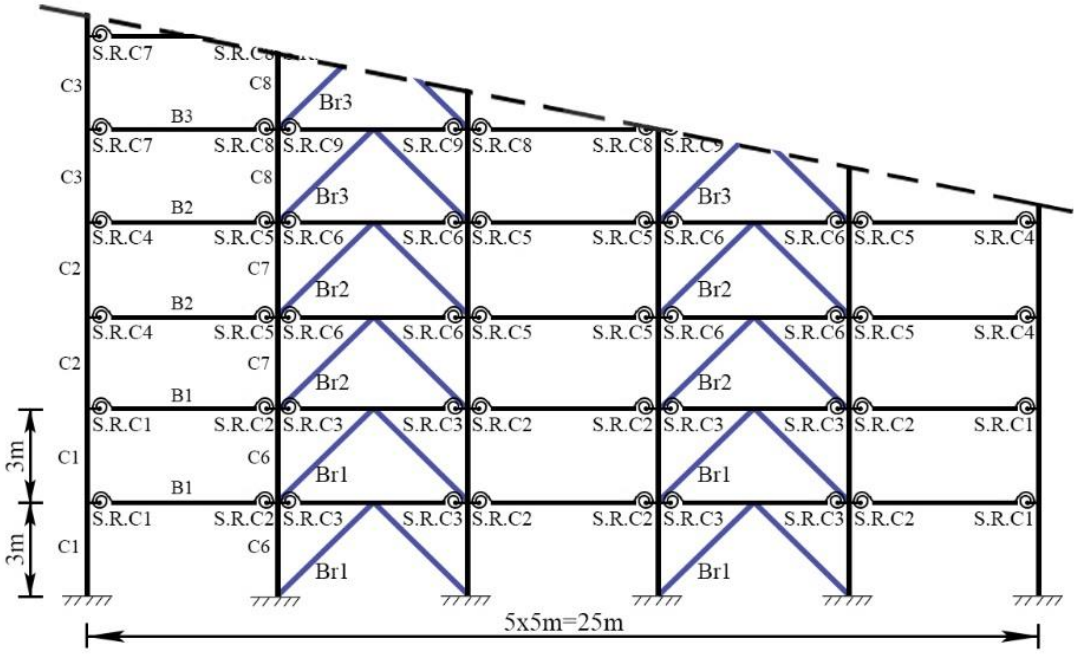

Figure 5: Dimensions and grouping of steel frame with chevron lateral bracing system with semi-rigid connections

Table 2: The available list of standard sections

Beams and Columns						braces			
No.	Profile	No.	Profile	No.	Profile	No.	Profile	No.	Profile
1	W14×22	11	W14×74	21	W14×193	31	HSS3×3×0.375	41	HSS9×9×0.625
2	W14×26	12	W14×82	22	W14×211	32	HSS3-1/2×3–1/2×0.375	42	HSS10×10×0.500
3	W14×30	13	W14×90	23	W14×233	33	HSS4×4×0.500	43	HSS10×10×0.625
4	W14×34	14	W14×99	24	W14×257	34	HSS4-1/2×4–1/2×0.500	44	HSS14×14×0.500
5	W14×38	15	W14×109	25	W14×283	35	HSS5×5×0.500	45	HSS14×14×0.625
6	W14×43	16	W14×120	26	W14×311	36	HSS6×6×0.500	46	HSS16×16×0.625
7	W14×48	17	W14×132	27	W14×342	37	HSS7×7×0.625	47	HSS18×18×0.625
8	W14×53	18	W14×145	28	W14×370	38	HSS8×8×0.500	48	HSS20×20×0.625
9	W14×61	19	W14×159	29	W14×398	39	HSS8×8×0.625	49	HSS22×22×0.625
10	W14×68	20	W14×176	30	W14×426	40	HSS9×9×0.500	50	HSS24×24×0.625

5.1. 10-story steel frame with chevron lateral bracing system

For the optimization of the 10-story steel frame with a chevron bracing system, using the modified dolphin optimization algorithm (MDE), the number of structures in each iteration of the algorithm is considered equal to 40, with 400 iterations. Using the center of mass optimization algorithm (CMO), the number of iterations is 400, and the number of structures in each iteration is also considered equal to 40. Using the modified newton metaheuristic algorithm (MNMA), the number of iterations is 400, and the number of structures in each

[DOI: 10.22068/ijoce.2026.16.1.663]

iteration is considered equal to 40 as well.

Table 3: Optimization results for a 10-story frame

	MNMA		CMO		MDE	
	Rigid connection	semi-rigid connections	Rigid connection	semi-rigid connections	Rigid connection	semi-rigid connections
C1	19	19	18	19	18	19
C2	17	19	17	18	16	17
C3	15	16	14	15	15	14
C4	12	13	13	13	12	12
C5	10	11	10	11	11	11
C6	18	19	17	18	17	18
C7	17	17	16	17	15	16
C8	15	16	15	15	15	15
C9	12	14	13	14	13	13
C10	10	10	10	11	11	10
B1	10	9	9	9	10	9
B2	9	9	10	9	9	8
B3	8	8	9	8	8	9
B4	8	7	8	8	8	8
B5	7	7	7	7	7	7
BR1	41	42	40	43	41	42
BR2	40	41	40	42	40	41
BR3	38	41	39	41	39	40
BR4	36	36	35	38	37	39
BR5	34	35	34	35	35	35
Weight(kg)	55073	57317	54596	56987	54568	55269
Cost ($)	90,796 $	87,701 $	90,721 $	87,547 $	90,139 $	84,784 $
Deviation from the standard	1286	1325	1106	1186	1026	1123
Percentage of best result	7.09%	3.44%	7.00%	3.25%	6.32%	--

In order to reach the optimal solution and avoid local optima, the optimization process with the above-mentioned number of iterations is repeated 10 times for each algorithm. Table 3 presents the structural sections according to Table 2 as well as the execution costs obtained by each algorithm. As can be seen from this table, the best statistical result is obtained by the (MDE) algorithm.

In Table. 4, the values of the rotational stiffness of the semi-rigid connections, obtained after the optimization process for the 10-story steel frame with a chevron bracing system, are presented by the algorithms. Fig. 6, shows the convergence curves for the 10-story frame. In Fig. 7, the pushover curves of the optimized 10-story frames with semi-rigid and rigid connections under the lateral load pattern according to $\boldsymbol{C_{vx}}$ (Equation 2) are shown.

The code-based constraints governing the design process of the 10-story frame include the inter-story drift constraint at the IO level, the axial deformation constraint of the braces at the IO level, the force-controlled column constraint $g_{FC.i}^{2/50}$ at the CP performance level, as well as the plastic rotation constraint of beams and columns at the CP level. Fig. 8, shows the values of the above constraints for the optimized frames with semi-rigid and rigid connections. As can be observed, all performance-based design constraints lie within the permissible range.

[DOI: 10.22068/ijoce.2026.16.1.663]

Table 4: Results of optimization of initial rotational stiffness of semi-rigid connections of 10-story frame

	MNMA	CMO	MDE
	KNm/rad	KNm/rad	KNm/rad
S.R.C1	191000	201000	181000
S.R.C2	201000	211000	201000
S.R.C3	221000	231000	221000
S.R.C4	201000	191000	171000
S.R.C5	181000	191000	181000
S.R.C6	201000	211000	201000
S.R.C7	171000	161000	141000
S.R.C8	171000	171000	151000
S.R.C9	181000	191000	181000
S.R.C10	131000	121000	101000
S.R.C11	141000	131000	111000
S.R.C12	131000	141000	141000
S.R.C13	111000	101000	91000
S.R.C14	101000	91000	81000
S.R.C15	121000	111000	101000

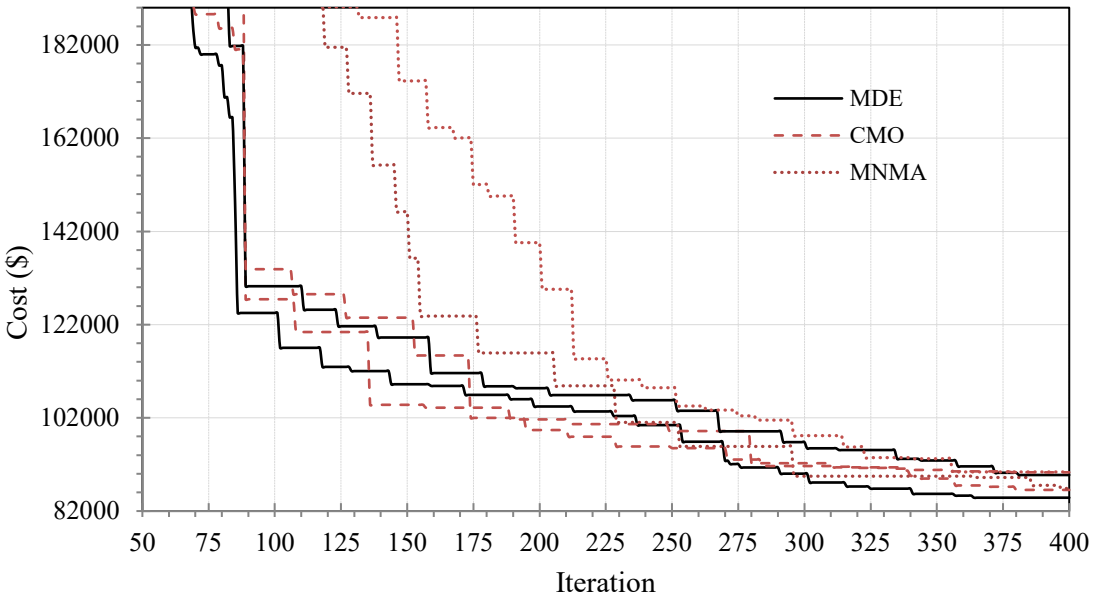

Figure 6: convergence curves for the 10-story frame.

5.2. 15-story steel frame with chevron lateral bracing system

For the optimization of the 15-story steel frame with a chevron bracing system, the modified dolphin optimization algorithm (MDE) was implemented with a population size of 40 structures per iteration and 500 iterations. Similarly, the center of mass optimization algorithm (CMO) was applied with 500 iterations and a population size of 40 structures per iteration, and the modified newton metaheuristic algorithm (MNMA) was also applied with 500 iterations and a population size of 40 structures per iteration. To obtain the optimal solution and avoid local optima, the optimization process with the above iteration numbers was repeated 10 times for each algorithm. Table 5 presents the structural sections (according

[DOI: 10.22068/ijoce.2026.16.1.663]

to Table 2) as well as the execution cost obtained by each algorithm. As can be observed from this table, the best statistical result was obtained using the MDE algorithm.

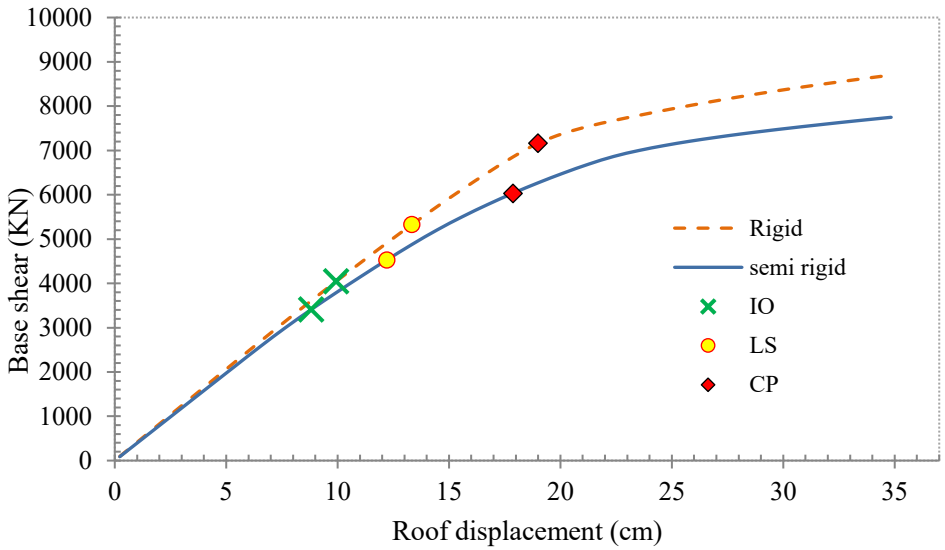

Figure 7: Pushover curve under the C_{vx} lateral load pattern for the 10-story structure

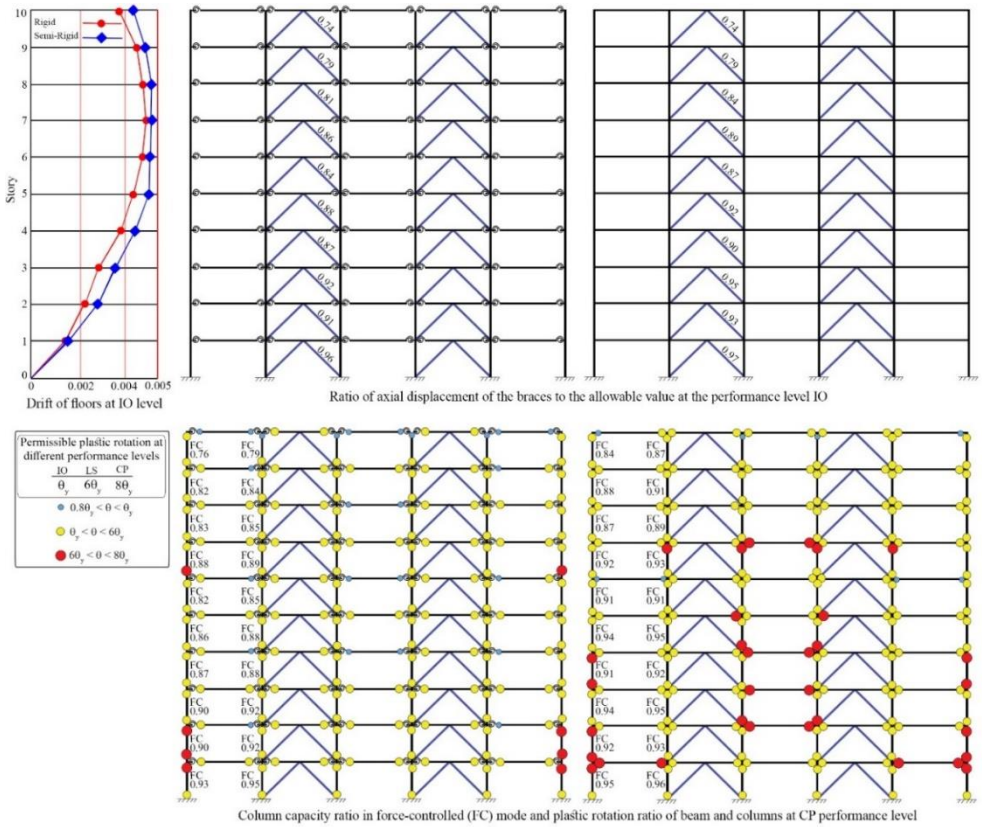

Figure 8: Active design constraints for optimal 10-story frames

[DOI: 10.22068/ijoce.2026.16.1.663]

In Table. 6, the values of the rotational stiffness of the semi-rigid connections, obtained after the optimization process for the 15-story steel frame with a chevron bracing system, are presented by the algorithms. Fig. 9, presents the convergence curves for the 15-story frame. In Fig. 10, the pushover curves of the optimized 15-story frames with semi-rigid and rigid connections under the lateral load pattern according to $\boldsymbol{C_{vx}}$ (Equation 2) are illustrated.

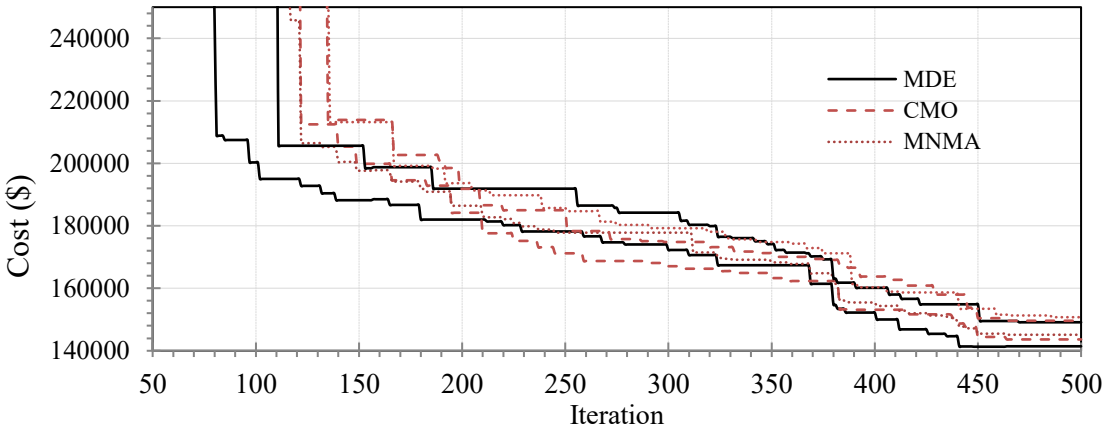

Figure 9: convergence curves for the 15-story frame

Table 5: Optimization results for a 15-story frame

	MNMA		CMO		MDE	
	Rigid connection	semi-rigid connections	Rigid connection	semi-rigid connections	Rigid connection	semi-rigid connections
C1	23	23	23	24	22	23
C2	22	23	22	22	21	21
C3	19	20	18	19	19	19
C4	19	19	17	17	17	16
C5	18	16	17	15	15	15
C6	15	13	15	14	15	15
C7	14	13	12	13	13	12
C8	11	11	11	11	10	11
C9	22	22	22	23	21	22
C10	21	21	20	21	20	20
C11	19	19	18	19	18	19
C12	17	19	18	18	18	18
C13	16	16	15	15	16	16
C14	14	15	14	14	14	15
C15	11	11	12	12	11	11
C16	10	10	10	10	10	10
B1	9	9	9	9	9	9
B2	8	9	8	8	8	9
B3	8	8	9	9	9	9
B4	8	8	9	9	9	8
B5	9	9	8	8	8	8
B6	8	8	9	9	9	9
B7	8	8	8	8	8	7
B8	7	7	7	7	7	7
BR1	42	41	42	43	43	44

[DOI: 10.22068/ijoce.2026.16.1.663]

BR2	41	41	40	40	41	42
BR3	40	39	40	39	40	40
BR4	39	38	38	38	39	39
BR5	36	37	34	35	35	35
BR6	34	34	33	34	34	34
BR7	33	34	33	34	33	34
BR8	33	33	32	33	32	33
Weight(kg)	95025	97113	93335	96129	92958	94540
Cost ($)	155,608 $	147,432 $	154,667$	146,346$	154,176$	143,493$
Deviation from the standard	1687	1825	1509	1786	1402	1628
Percentage of best result	8.44%	2.74%	7.79%	1.99%	7.45%	--

The code-based constraints governing the design process of the 15-story frame include the story drift constraint at the IO level, the axial deformation constraint of the braces at the IO level, the column force-controlled constraint $g_{FC.i}^{2/50}$ at the CP performance level, as well as the plastic rotation constraint of beams and columns at the CP level. Fig. 11, shows the values of these constraints for the optimized frames with semi-rigid and rigid connections. As observed, all performance-based design constraints remain within the allowable limits.

Table 6: Results of optimization of initial rotational stiffness of semi-rigid connections of 15-story frame

	MNMA	CMO	MDE
	kNm/rad	kNm/rad	kNm/rad
S.R.C1	241000	241000	251000
S.R.C2	231000	221000	231000
S.R.C3	211000	201000	211000
S.R.C4	241000	241000	241000
S.R.C5	241000	231000	221000
S.R.C6	201000	201000	201000
S.R.C7	241000	231000	221000
S.R.C8	211000	211000	201000
S.R.C9	201000	191000	191000
S.R.C10	221000	211000	201000
S.R.C11	211000	201000	191000
S.R.C12	191000	191000	181000
S.R.C13	211000	201000	191000
S.R.C14	191000	181000	181000
S.R.C15	171000	171000	161000
S.R.C16	201000	191000	201000
S.R.C17	191000	181000	191000
S.R.C18	191000	191000	191000
S.R.C19	221000	211000	201000
S.R.C20	191000	181000	191000
S.R.C21	181000	181000	181000
S.R.C22	191000	181000	191000
S.R.C23	171000	161000	181000
S.R.C24	161000	161000	181000

[DOI: 10.22068/ijoce.2026.16.1.663]

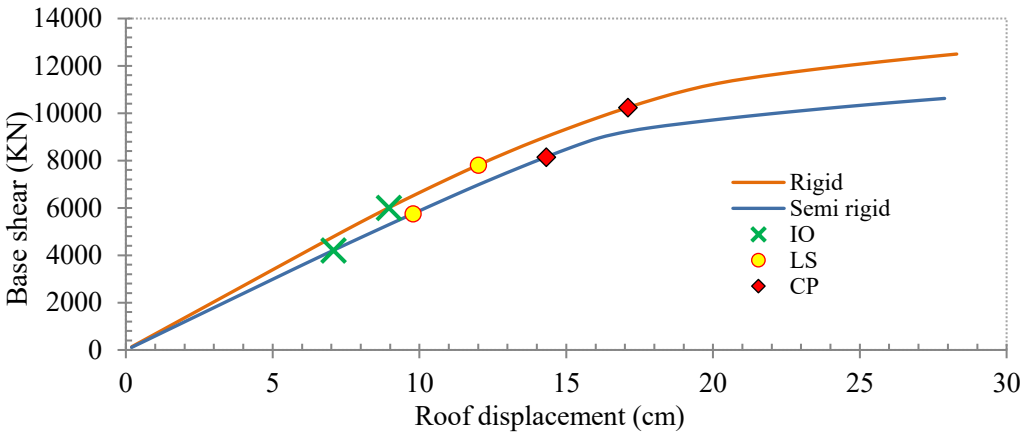

Figure 10: Pushover curve under the C_{vx} lateral load pattern for the 15-story structure

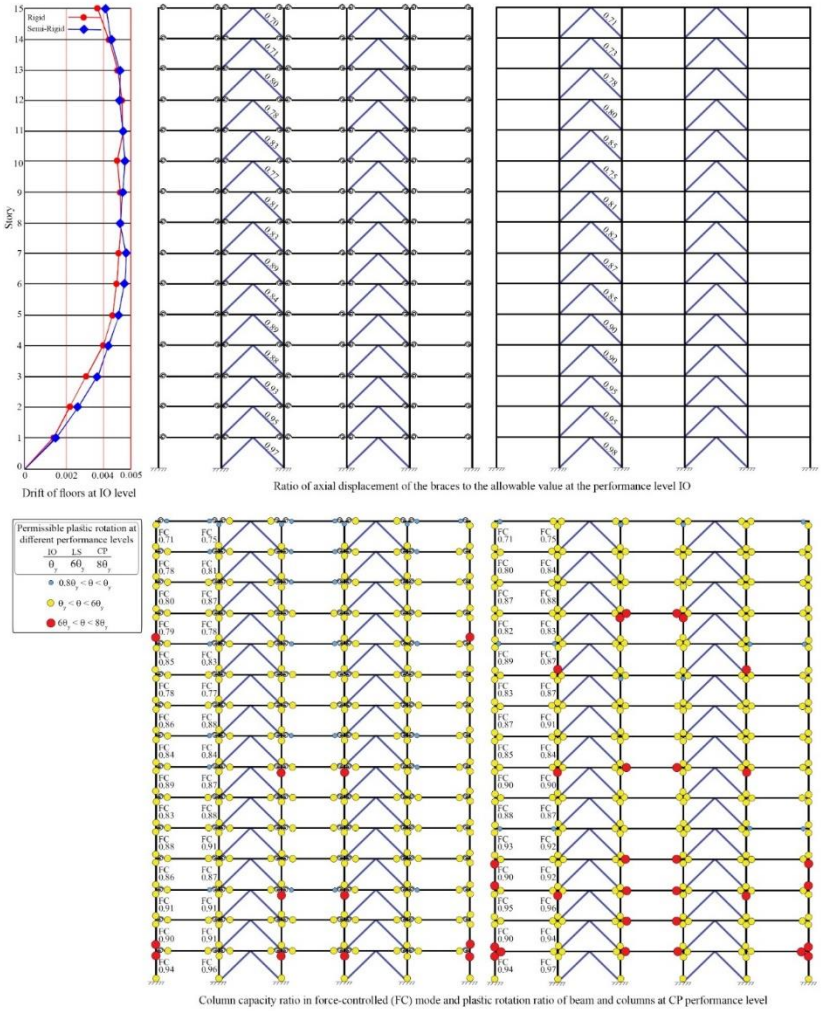

Figure 11: Active design constraints for optimal 15-story frames

[DOI: 10.22068/ijoce.2026.16.1.663]

7. CONCLUSIONS

This study demonstrated the effectiveness of metaheuristic algorithms in addressing complex structural optimization problems involving nonlinear behavioral variables. By integrating metaheuristic optimization with performance-based design and explicitly considering the realistic behavior of semi-rigid connections, optimized structural configurations were developed, providing a novel framework for the cost- and performance-efficient design of steel chevron-braced frames.

For this purpose, 10- and 15-story chevron-braced steel frames were optimized using three different algorithms. In the optimization procedure, the initial rotational stiffness of beam-to-column connections was first treated as a key design variable. To enable comparison, all connections were also modeled as rigid in a separate set of analyses. The choice of algorithms was informed by their previously demonstrated capability in solving similar classes of nonlinear optimization problems.

The results highlight the substantial influence of connection stiffness on construction cost. Using the MDE algorithm, this effect translated to a 6–7% variation in the optimal cost of the steel frames. Furthermore, the comparative analysis confirmed the superior performance of the MDE algorithm over the other approaches.

For the 10-story frame, MDE yielded the most efficient design, achieving a 3.25% lower optimal cost than CMO and a 3.44% lower cost than MNMA for semi-rigid connections. Similar improvements were observed for rigid connections, where MDE consistently provided the lowest costs. For the 15-story frame, the advantage of MDE was again evident: it delivered 1.99% lower costs compared to CMO and 2.74% lower costs compared to MNMA for semi-rigid connections, and maintained its superiority in the rigid connection case as well.

Overall, these findings emphasize the critical role of considering connection flexibility in cost-optimal structural design and demonstrate the robustness of metaheuristic algorithms, particularly MDE, in navigating the nonlinear design space. An efficient optimization algorithm not only minimizes construction cost but also ensures compliance with all performance-based design constraints, pushing them simultaneously to their allowable limits, thereby delivering the most economical and resilient structural solution.

[DOI: 10.22068/ijoce.2026.16.1.663]

REFERENCES

1. Kaveh A, Farahmand Azar B, Hadidi A, Rezazadeh Sorochi F, Talatahari S. Performance-based seismic design of steel frames using ant colony optimization. *J Constr Steel Res* 2010;**66**:566–74.
2. Rao SS. Engineering optimization: theory and practice. Hoboken: John Wiley & Sons; 2009.
3. Razavi M, Sheidaii MR. Seismic performance of cable zipper-braced frames. *J Constr Steel Res* 012;**74**:49–57.
4. Liu D, Zheng Y, Wang Z, Pan J, Hu F, Yin T. Boundary-oriented optimization of semi-rigid connections in steel frames using BNSGA. *J Constr Steel Res* 2024;**214**:108471.

5. AISC. Specification for structural steel buildings. Chicago: American Institute of Steel Construction; 2010.
6. Eurocode 3. Design of steel structures, Part 1-8: Design of joints. EN 1993-1-8. Brussels: European Committee for Standardization; 2005.
7. GB 50017-2017. Standard for design of steel structures. Beijing: CABP; 2017.
8. Liu D, Wang Z, Pan J, Zheng Y, Hu Z. Optimum design of nonlinear semi-rigid steel frame based on performance-price ratio via genetic algorithm. *J Build Eng* 2022;**61**:105287.
9. Qiu Y, Wang Z, Pan J, Hu F. Optimal design of semi-rigid connection steel frame with infilled shear walls using dolphin echolocation algorithm. *Structures* 2023;**57**:104955.
10. Machaly ESB. Optimum weight analysis of steel frames with semirigid connections. *Comput Struct* 1986;**23**(4):461–74.
11. Simões LMC. Optimization of frames with semi-rigid connections. *Comput Struct* 1996;**60**(4):531–9.
12. Xu L, Grierson DE. Computer-automated design of semirigid steel frameworks. *J Struct Eng* 1993;**119**(6):1740–60.
13. Kameshki ES, Saka MP. Optimum design of nonlinear steel frames with semi-rigid connections using a genetic algorithm. *Comput Struct* 2001;**79**(17):1593–604.
14. Kameshki ES, Saka MP. Genetic algorithm based optimum design of nonlinear planar steel frames with various semi-rigid connections. *J Constr Steel Res* 2003;**59**(1):109–34.
15. Hayalioglu MS, Degertekin SO. Design of non-linear steel frames for stress and displacement constraints with semi-rigid connections via genetic optimization. *Struct Multidiscip Optim* 2004;**27**(4):259–71.
16. Hayalioglu MS, Degertekin SO. Minimum cost design of steel frames with semi-rigid connections and column bases via genetic optimization. *Comput Struct* 2005;**83**(21):1849–63.
17. Hagishita T, Ohsaki M. Optimal placement of braces for steel frames with semi-rigid joints by scatter search. *Comput Struct* 2008;**86**(21–22):1983–93.
18. Bel Hadj Ali N, et al. Multi-stage production cost optimization of semi-rigid steel frames using genetic algorithms. *Eng Struct* 2009;**31**(11):2766–78.
19. Hadidi A, Rafiee A. A new hybrid algorithm for simultaneous size and semi-rigid connection type optimization of steel frames. *Int J Steel Struct* 2015;**15**(1):89–102.
20. Artar M, Daloğlu AT. Optimum design of composite steel frames with semi-rigid connections and column bases via genetic algorithm. *Steel Compos Struct* 2015;**19**(4):1035–53.
21. Artar M, Daloğlu AT. Optimum weight design of steel space frames with semi-rigid connections using harmony search and genetic algorithms. *Neural Comput Appl* 2018;**29**(11):1089–100.

[DOI: 10.22068/ijoce.2026.16.1.663]

22. Shallan O, et al. Design optimization of semi-rigid space steel frames with semi-rigid bases using biogeography-based optimization and genetic algorithms. *Struct Eng Mech* 2019;**70**(2):221–31.
23. Truong VH, et al. An efficient method for optimizing space steel frames with semi-rigid joints using practical advanced analysis and the micro-genetic algorithm. *J Constr Steel Res* 2017;**128**:416–27.
24. Truong VH, Kim S. An efficient method for reliability-based design optimization of nonlinear inelastic steel space frames. *Struct Multidiscip Optim* 2017;**56**(2):331–51.
25. FEMA. Prestandard and commentary for the seismic rehabilitation of buildings (FEMA 356). Washington: Federal Emergency Management Agency; 2000.
26. ASCE/SEI. Seismic evaluation and retrofit of existing buildings. Reston: American Society of Civil Engineers; 2017.
27. ANSI/AISC 360-22. Specification for structural steel buildings. Chicago: American Institute of Steel Construction; 2022.
28. Kunnath SK. Identification of modal combinations for nonlinear static analysis of building structures. *Comput Aided Civ Infrastruct Eng* 2004;**19**:282–95.
29. Kishi N, Chen WF. Moment-rotation relations of semi-rigid connections with angles. *J Struct Eng* 1990;**116**(7):1813–34.
30. Moghaddam H, Sadrara A. Experimental and numerical evaluation of the mechanical characteristics of semi-rigid saddle connections. *Struct Design Tall Spec Build* 2022;**31**(7):e1923.
31. Moghaddam H, Sadrara A. Improving the mechanical characteristics of semi-rigid saddle connections. *J Constr Steel Res* 2021;**186**:106917.
32. Qin J, Wang Z, Pan J, Li B, Fan Y. Moment–rotation curve characteristics and initial rotational stiffness calculation method of angle connections. *Struct Design Tall Spec Build* 2022;**31**(3):e1906.
33. Zhang AL, Li C, Zhang YX, Liu XC. Experimental and theoretical analyses on semi-rigid pin joints under in-plane direction bending in modular reticulated shell. *J Constr Steel Res* 2022;**190**:107128.
34. Azizinamini A, Bradburn J, Radziminski J. Initial stiffness of semi-rigid steel beam-to-column connections. *J Constr Steel Res* 1987;**8**:71–90.
35. Brown N, Anderson D. Structural properties of composite major axis end plate connections. *J Constr Steel Res* 2001;**57**(3):327–49.
36. Uriz P, Mahin A. Toward earthquake-resistant design of concentrically braced steel-frame structures. Berkeley: PEER; 2008.
37. Krawinkler H. Shear in beam-column joints in seismic design of steel frames. J Struct Div ASCE 1978.
38. Gupta A, Krawinkler H. Seismic demands for performance evaluation of steel moment resisting frame structures. Stanford: Blume Center Report; 1999.

[DOI: 10.22068/ijoce.2026.16.1.663]

39. Astaneh-Asl A. Seismic behavior and design of steel panel zones. Moraga: Structural Steel Educational Council; 2000.
40. Kim J, Choi H, Chung L. Joint behavior effects on seismic performance of steel frames. J Constr Steel Res 2001.
41. Lee K, Foutch DA. Performance evaluation of new steel frame buildings for seismic loads. Earthq Eng Struct Dyn 2002.
42. Kishi N, Chen WF. Moment-rotation relations of semi-rigid connections with angles. *J Struct Eng* 1990;**116**(7):1813–34.
43. Jaspart JP. Contributions to recent developments in the field of steel joints. *J Constr Steel Res* 1997;**43**(1–3):95–123.
44. Song Y, Zhang M, Ke K, Yam MCH, Lin XM. Behaviour and design of gusset plates in steel structures: A state of the art review. *J Constr Steel Res* 2023;**211**:108188.
45. Chen WF, Lui EM. Structural stability: theory and implementation. Boca Raton: CRC Press; 2006.
46. Surovek AE, Gusset TM. Evaluation of gusset plate behavior and modeling techniques. *J Constr Steel Res* 2005;**61**(10):1446–62.
47. Kishi N, Chen WF. Moment–rotation relations of semi-rigid connections with angle, T-stub, and end-plate connections. *J Constr Steel Res* 1990;**18**(3):197–218. https://doi.org/10.1016/0143-974X(90)90005-Z.
48. Gholizadeh S, Ebadijalal M. Performance based discrete topology optimization of steel braced frames by a new metaheuristic. *Adv Eng Softw* 2018;**123**:77–92.
49. Nabati M, Gholizadeh S. Performance-based optimization of steel moment frames by a modified Newton metaheuristic algorithm. *Int J Optim Civil Eng* 2023;**13**(2):177–88.
50. Kaveh A, Farhoudi N. A new optimization method: dolphin echolocation. *Adv Eng Softw* 2013;**59**:53–70.
51. Kaveh A, Zaerreza A. Shuffled shepherd optimization method: a new meta-heuristic algorithm. *Eng Comput* 2020;**37**:2357–89.
52. Truong VH, Nguyen PC, Kim SE. An efficient method for optimizing space steel frames with semi-rigid joints using practical advanced analysis and the micro-genetic algorithm. *J Constr Steel Res* 2017;**125**:416–27.
53. OpenSees version 2.4.0 [computer software]. Berkeley: PEER; n.d.
54. MATLAB. The language of technical computing. Natick: MathWorks; 2024.

[DOI: 10.22068/ijoce.2026.16.1.663]